

High-Spin Doublet Band Structures in odd-odd $^{194-200}\text{Tl}$ isotopes

S. Jehangir^{a,4}, I. Maqbool², G.H. Bhat^{b,1,3}, J.A. Sheikh^{c,2,3}, R. Palit⁴, N. Rather⁵

¹Department of Physics, SP College Srinagar, Jammu and Kashmir, 190 001, India

²Department of Physics, University of Kashmir, Srinagar, 190 006, India

³Cluster University Srinagar, Jammu and Kashmir, Srinagar, Goji Bagh, 190 008, India

⁴Department of Nuclear and Atomic Physics, Tata Institute of Fundamental Research, Mumbai - 400 005, India

⁵Department of Physics, Islamic University of Science and Technology, Jammu and Kashmir, 192 122, India

Received: date / Accepted: date

Abstract The basis space in the triaxial projected shell model (TPSM) approach is generalized for odd-odd nuclei to include two-neutron and two-proton configurations on the basic one-neutron coupled to one-proton quasiparticle state. The generalization allows to investigate odd-odd nuclei beyond the band crossing region and as a first application of this development, high-spin band structures recently observed in odd-odd $^{194-200}\text{Tl}$ isotopes are investigated. In some of these isotopes, the doublet band structures observed after the band crossing have been conjectured to arise from the spontaneous breaking of the chiral symmetry. The driving configuration of the chiral symmetry in these odd-odd isotopes is one-proton and three-neutrons rather than the basic one-proton and one-neutron as already observed in many other nuclei. It is demonstrated using the TPSM approach that energy differences of the doublet bands in ^{194}Tl and ^{198}Tl are, indeed, small. However, the differences in the calculated transition probabilities are somewhat larger than what is expected in the chiral symmetry limit. Experimental data on the transition probabilities is needed to shed light on the chiral nature of the doublet bands.

Keywords Chiral bands, triaxial nuclei, signature inversion

PACS 2

1.60.Cs, 21.10.Hw, 21.10.Ky, 27.50.+e

1 Introduction

High-spin spectroscopy has played a pivotal role to unravel the structure of atomic nuclei at high angular momentum and excitation energy [1]. The advancements in the spectroscopic techniques have allowed to probe the properties of

nuclei in regions that were hitherto inaccessible. The band structures have been identified up to very high angular momentum and excitation energy and data has revealed interesting phase and shape transitions [2]. In odd-odd nuclei, the energy spectrum is quite rich as compared to even-even and odd-mass nuclei due to extra neutron-proton coupling. Recently, in odd-odd $^{194-200}\text{Tl}$ isotopes, band structures have been populated beyond the first band crossing and it has been speculated that near degeneracy of the yrast and the side band energies, observed in some of these isotopes, may be a consequence of the chiral symmetry breaking mechanism [3, 4, 5, 6]. In these isotopes, band structures have one-proton and three-neutron, $\pi h_{9/2} \otimes \nu i_{13/2}^{-3}$ configuration at higher spins and one-proton and one-neutron, $\pi h_{9/2} \otimes \nu i_{13/2}^{-1}$ configuration at lower spins.

Chiral symmetry has been studied quite extensively in triaxial deformed nuclei [7, 8, 9, 10]. In the original work, the chiral symmetry mechanism was proposed for odd-odd nuclei with the angular-momentum of the odd-proton and odd-neutron aligned towards short- and long-axis, and the angular-momentum of the deformed core projected towards the intermediate axis [11]. As the clock-wise and the counter clock-wise rotation of the three orthogonal vectors are equivalent, this results into doublet band structures with identical spectroscopic properties. Doublet bands with similar properties have been observed in several mass regions of the periodic table [12, 13, 14, 15, 16], including the $A \sim 80$ region in recent works [17, 18, 19]. Chiral symmetry breaking has also been proposed in odd-mass [16, 20] and even-even nuclei [21]. Theoretically, several nuclear models have been employed to investigate the chiral symmetry breaking mechanism, which include both microscopic and phenomenological models [22, 23, 24, 25, 26]. Triaxial projected shell model (TPSM) approach, a semi-microscopic model, has been used to elucidate the band structures in deformed and transitional

^ae-mail: sheikhahmad.phy@gmail.com

^be-mail: gwhr.bhat@gmail.com

^ce-mail: sjaphysics@gmail.com

nuclei [27]. It has been demonstrated that the properties of the observed doublet bands are reproduced quite successfully using the TPSM approach [28]. The advantage of the TPSM approach is that computational needs are quite modest and it is possible to perform systematic studies in a reasonable time frame. As a matter of fact several systematic studies have been performed using the TPSM approach [29, 30, 31, 32, 33].

For odd-odd nuclei, the basis space in the TPSM approach is composed of one-neutron coupled to one-proton quasiparticle configurations [28]. This basis space is obviously quite restrictive and allows to study only low-lying states in odd-odd nuclei. To study high-spin states in odd-odd nuclei, around and beyond the band crossing, it is imperative to include two-neutron and two-proton states coupled to the basic one-neutron plus one-proton states. This extension of the model space will allow to probe the high-spin band structures beyond the first band crossing. In the present work, the model space has been expanded to include two-neutron and two-proton quasiparticle configuration over the primary one-proton plus one-neutron configuration. As a first application of this development, the properties of the observed band structures in odd-odd $^{194-200}\text{Tl}$ nuclei are investigated. In these isotopes, doublet band structures, observed above first band crossing having four-quasiparticle configuration, are predicted to originate from the chiral symmetry breaking mechanism. These shall be first examples of the manifestation of chiral symmetry in odd-odd with four-quasiparticle structures. In all earlier studies of odd-odd nuclei, chiral bands have been identified with one-proton and one-neutron configuration. The present work is organised in the following manner. In the next section, the TPSM approach is presented with the expanded model space. In section III, the results are presented and discussed. Finally, the present work is summarized and concluded in section IV.

2 Triaxial Projected Shell Model Approach

In recent years, the triaxial projected shell model approach has been shown to reproduce the properties of deformed odd-odd nuclei quite well. In the earlier version, the basis space for odd-odd nuclei was composed of one-neutron coupled to one-proton only [28]. In the present work, the basis space is generalized to include two-neutron and two-proton quasiparticle configurations coupled to the basic one-neutron \otimes one-proton configuration. The generalized TPSM basis space is given by :

$$\begin{aligned} & \hat{P}_{MK}^I a_{v_1}^\dagger a_{\pi_1}^\dagger | \Phi \rangle; \\ & \hat{P}_{MK}^I a_{v_1}^\dagger a_{v_2}^\dagger a_{v_3}^\dagger a_{\pi_1}^\dagger | \Phi \rangle; \\ & \hat{P}_{MK}^I a_{v_1}^\dagger a_{\pi_1}^\dagger a_{\pi_2}^\dagger a_{\pi_3}^\dagger | \Phi \rangle, \end{aligned} \quad (1)$$

where \hat{P}_{MK}^I is the three-dimensional angular-momentum-projection operator [34]. The triaxial quasi-particle (qp) vac-

uum configuration, $|\Phi\rangle$, in Eq. (1) is constructed through diagonalization of the deformed Nilsson Hamiltonian and a subsequent BCS calculations. This provides the triaxial qp-basis in the present model.

The intrinsic states generated from the deformed Nilsson calculations don't conserve rotational symmetry. To restore this symmetry, three-dimensional angular-momentum projection technique is applied. From each intrinsic state, a band is generated through projection technique as discussed in Refs. [35, 36]. The interaction between different bands with a given spin is taken into account by diagonalising the shell model Hamiltonian in the projected basis. The Hamiltonian used in the present work is given by

$$\hat{H} = \hat{H}_0 - \frac{1}{2} \chi \sum_{\mu} \hat{Q}_{\mu}^{\dagger} \hat{Q}_{\mu} - G_M \hat{P}^{\dagger} \hat{P} - G_Q \sum_{\mu} \hat{P}_{\mu}^{\dagger} \hat{P}_{\mu}, \quad (2)$$

with the corresponding mean-field (triaxial Nilsson) Hamiltonian

$$\hat{H}_N = \hat{H}_0 - \frac{2}{3} \hbar \omega \left\{ \beta \cos \gamma \hat{Q}_0 + \beta \sin \gamma \frac{\hat{Q}_{+2} + \hat{Q}_{-2}}{\sqrt{2}} \right\}, \quad (3)$$

In the above equations, \hat{H}_0 is the spherical single-particle Nilsson Hamiltonian [37]. The parameters of the Nilsson potential are fitted to a broad range of nuclear properties and is employed as a mean-field potential. The QQ-force strength, χ , in Eq. (2) is adjusted such that the physical quadrupole deformation β is obtained as a result of the self-consistent mean-field HFB condition. The relation is given by [38]:

$$\chi_{\tau\tau'} = \frac{\frac{2}{3} \varepsilon \hbar \omega_{\tau} \hbar \omega_{\tau'}}{\hbar \omega_n \langle \hat{Q}_0 \rangle_n + \hbar \omega_p \langle \hat{Q}_0 \rangle_p}, \quad (4)$$

where $\omega_{\tau} = \omega_0 a_{\tau}$, with $\hbar \omega_0 = 41.4678A^{-\frac{1}{3}}$ MeV, and the isospin-dependence factor a_{τ} is defined as

$$a_{\tau} = \left[1 \pm \frac{N-Z}{A} \right]^{\frac{1}{3}}, \quad (5)$$

with $+$ ($-$) for $\tau =$ neutron (proton). It is to be noted that the strengths in the TPSM are fixed as in the original projected shell model approach with axial symmetry. The monopole pairing strength G_M (in MeV) is of the standard formas:

$$G_M = \left(G_1 \mp G_2 \frac{N-Z}{A} \right) \frac{1}{A} \text{ (MeV)}, \quad (6)$$

where $-(+)$ sign applies to neutrons (protons). In the present calculations, the pairing strength parameters, $G_1 = 20.12$ and $G_2 = 13.13$, are adopted so that the observed odd-even mass differences are reproduced with the model space of three active shells for neutrons and protons. The active shells considered are $N = 3, 4, 5$ for protons $N = 4, 5, 6$ for neutrons. The Nilsson parameters κ and μ for the major harmonic oscillator shells have been adopted from Zhang et al. [39] for the present set of calculations, and are listed in Table 1. The quadrupole pairing strength G_Q is assumed to be

Table 1 Set of Nilsson parameters used in the present calculation for odd-odd $^{194-200}\text{Tl}$ -isotopes.

Major Shell (N)	κ_π	μ_π	κ_ν	μ_ν
3	0.090	0.300	-	-
4	0.065	0.570	0.070	0.390
5	0.060	0.540	0.062	0.430
6	-	-	0.062	0.340

Table 2 The deformation parameters (β, γ) employed in the calculation for odd-odd $^{194-200}\text{Tl}$ -isotopes. The deformation parameters have been taken from Refs. [3, 4, 5, 6].

	^{194}Tl	^{196}Tl	^{198}Tl	^{200}Tl
β	0.178	0.168	0.157	0.157
γ	30	29	31	34

proportional to G_M and the proportionality constant being fixed as 0.16. These parameters are similar to those used in the earlier studies [29, 30].

In the present study, we have also evaluated the transition probabilities using the TPSM wavefunctions. The reduced electric quadrupole transition probability $B(E2)$ from an initial state (σ_i, I_i) to a final state (σ_f, I_f) is given by [40]

$$B(E2, I_i \rightarrow I_f) = \frac{e^2}{2I_i + 1} |\langle \sigma_f, I_f | \hat{Q}_2 | \sigma_i, I_i \rangle|^2. \quad (7)$$

In the calculations, we have used the effective charges of 1.6e for protons and 0.6e for neutrons. The reduced magnetic dipole transition probability $B(M1)$ is computed through

$$B(M1, I_i \rightarrow I_f) = \frac{\mu_N^2}{2I_i + 1} |\langle \sigma_f, I_f | \hat{\mathcal{M}}_1 | \sigma_i, I_i \rangle|^2, \quad (8)$$

where the magnetic dipole operator is defined as

$$\hat{\mathcal{M}}_1^\tau = g_l^\tau \hat{j}^\tau + (g_s^\tau - g_l^\tau) \hat{s}^\tau. \quad (9)$$

Here, τ is either ν or π , and g_l and g_s are the orbital and the spin gyromagnetic factors, respectively. In the calculations we use for g_l the free values and for g_s the free values damped by 0.85 factor, i.e.,

$$\begin{aligned} g_l^\pi &= 1, & g_l^\nu &= 0, & g_s^\pi &= 5.586 \times 0.85, \\ g_s^\nu &= -3.826 \times 0.85. \end{aligned} \quad (10)$$

The reduced matrix element of an operator $\hat{\mathcal{O}}$ ($\hat{\mathcal{O}}$ is either \hat{Q} or $\hat{\mathcal{M}}$) is given by

$$\begin{aligned} \langle \sigma_f, I_f | \hat{\mathcal{O}} | \sigma_i, I_i \rangle &= \sum_{\kappa_i, \kappa_f} f_{I_i \kappa_i}^{\sigma_i} f_{I_f \kappa_f}^{\sigma_f} \\ &\times \sum_{M_i, M_f, M} (-)^{I_f - M_f} \begin{pmatrix} I_f & L & I_i \\ -M_f & M & M_i \end{pmatrix} \\ &\times \langle \phi_{\kappa_f} | \hat{P}_{\kappa_f M_f}^{I_f} \hat{\mathcal{O}}_{LM} \hat{P}_{\kappa_i M_i}^{I_i} | \phi_{\kappa_i} \rangle. \end{aligned} \quad (11)$$

3 Results and Discussions

TPSM calculations have been performed for odd-odd $^{194-200}\text{Tl}$ isotopes with the deformation parameters listed in Table 2. The axial and non-axial deformation values have been adopted from [3, 4, 5, 6]. Quasiparticle states are generated with these deformation values by performing Nilsson plus BCS calculations. The quasiparticle configurations close to the Fermi surface for each system are then projected onto states with good angular momentum by performing three-dimensional angular momentum projection [34]. As an illustrative example, the lowest projected bands are displayed in Fig. 1 for ^{194}Tl . For other three isotopes, the projected bands have a similar behaviour and are not discussed. The ground state band for ^{194}Tl in Fig. 1 is the projected band with $K=4$ from one-proton coupled to one-neutron quasiparticle configuration having quasiparticle energy of 1.9 MeV. This two quasiparticle configuration is crossed at $I=16$ by two-neutron aligned state coupled to one-proton \otimes one-neutron configuration having $K=4$ with quasiparticle energy of 3.5 MeV.

The lowest projected bands, shown in Fig. 1, and many more bands close to the Fermi surface, which are about 40 for each nucleus, are then used to diagonalize the shell model Hamiltonian of Eq. 2. The calculated lowest two bands, referred to as yrast and the side-bands, are displayed in Fig. 2 for the studied Tl isotopes. The available experimental data is also shown in the figure for comparison. For ^{194}Tl , the data for both the bands is available up to quite high spin and it is evident from Fig. 2 that TPSM calculations reproduce the experimental results reasonably well. It is noted that deviation for the highest observed $I=24$ state is only about 100 keV. The two observed bands have similar excitation energies and have been proposed as a result of the chiral breaking mechanism. This shall be discussed in the following when analysing the differences in energies and transition probabilities of the two bands in detail.

For ^{196}Tl , the calculated yrast band is in good agreement with the experimental data with the maximum deviation for $I=20$ state being 235 keV. The side band has not been observed for this system and it is evident from the TPSM results that the predicted side band deviates from the yrast band quite substantially as compared to ^{194}Tl . In the case of ^{198}Tl , shown in Fig. 2, yrast band is observed up to $I=20$ and the side band only up to $I=14$. The TPSM calculations are again noted to reproduce the data quite well up to the highest observed spin. It is noted from the TPSM results that energy difference of the two bands tend to decrease somewhat with increasing spin. The yrast band in ^{200}Tl is observed up to $I=22$ and only three states have been populated for the side band. TPSM results reproduce the data fairly well.

To probe the crossing features of the observed band structures, the aligned angular momentum (i_x) for the yrast

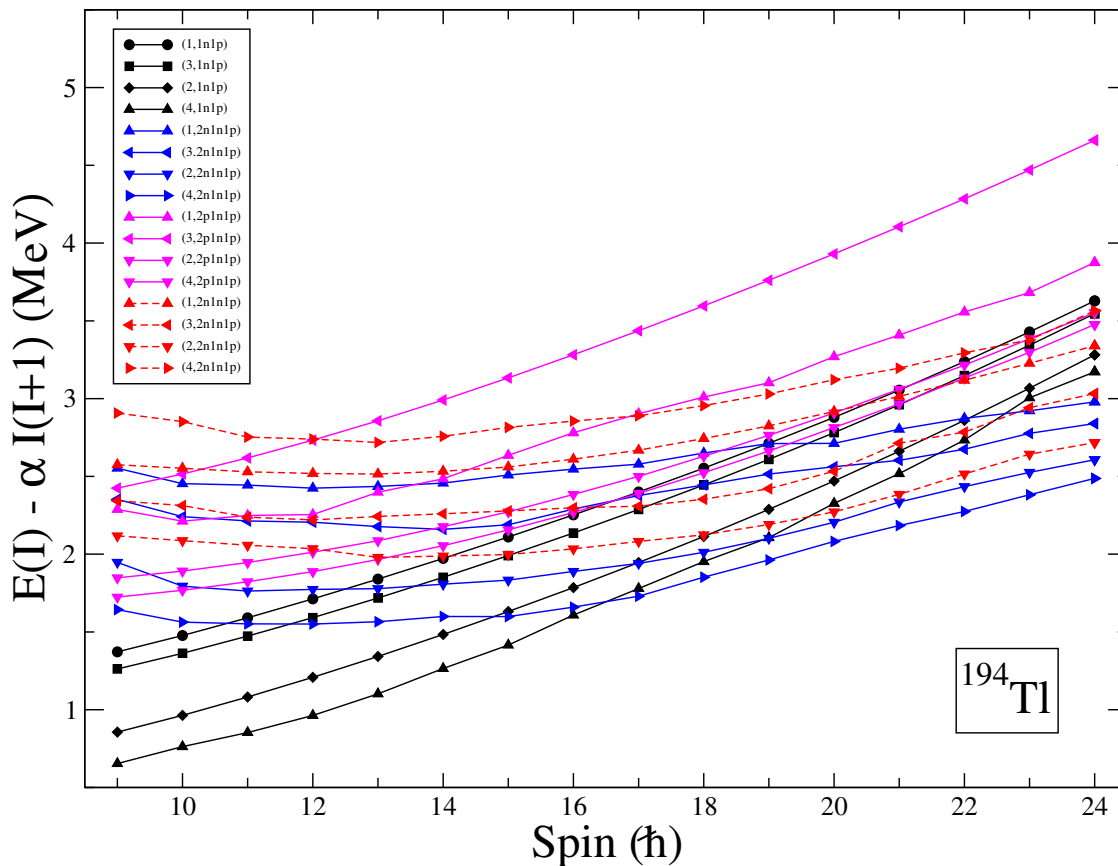


Fig. 1 (Color online) TPSM projected energies, before band mixing, of negative parity states for ^{194}Tl . Bands are labelled by $(K, \#)$ that designate the states with K quantum number and $\#$ the number of quasiparticles. For instance, $(1,1n1p)$, $(2,1n1p)$, $(3,1n1p)$, $(4,1n1p)$ correspond to the $K = 1, 2, 3, 4$ one-neutron coupled to one-proton quasiparticle state. The value of α , shown in y-axis, is defined as $\alpha = 32.32A^{-5/3}$.

and the side bands are displayed in Figs. 3 and 4. It is apparent from the results that TPSM calculations are in good agreement with the calculated values from the experimental data. In all the studied Tl-isotopes, the crossing is observed around $0.3\hbar\omega$ and is due to the alignment of two-neutrons. This is evident from Fig. 1 with the configuration having two-neutron coupled to one-proton \otimes one-neutron crossing the ground-state band.

Further, deformed odd-odd nuclei in most of the regions of the periodic table are known to depict signature inversion in the low-spin regime. Considerable efforts have been devoted to understand the nature of the signature inversion. It has been demonstrated that residual neutron-proton interaction and triaxility can lead to signature inversion [41]. To analyze whether TPSM calculations are able to reproduce it, the energy staggering defined by $S(I) = \frac{[E(I) - E(I-1)]}{(2I)}$ for the yrast bands are shown in Fig. 5. It is noted from the figure that TPSM approach is able to reproduce the observed signature inversion in ^{194}Tl without introducing any residual interaction. In other studies [3, 4, 5, 6], additional J-dependent

neutron-proton interaction has been introduced to reproduce the signature inversion. For other Tl-isotopes, it is seen that TPSM results depict a little delayed inversion point. However, the magnitude of the signature splitting is reproduced fairly well for the intermediate spin values and some deviation is noted at high spin for ^{194}Tl . The delayed signature inversion in $^{196-200}\text{Tl}$ isotopes needs further studies and in future we are planning to perform a detailed analysis of the signature inversion in this mass region and other regions using the TPSM approach.

In the present work, we have also performed a detailed investigation of the transition probabilities for the studied four Tl-isotopes. The effective charges used and other relevant information have been presented in section II. The calculated $B(E2)$ and $B(M1)$ transitions are displayed in Figs. 6 and 7, respectively. Unfortunately, except for ^{194}Tl , there is no experimental data to compare with and we hope that data shall become available in the near future.

The data for the $B(M1)/B(E2)$ ratios is available for some bands and are depicted in Figs. 8 and 9 with the calculated TPSM values. For ^{194}Tl , ratios are available for both

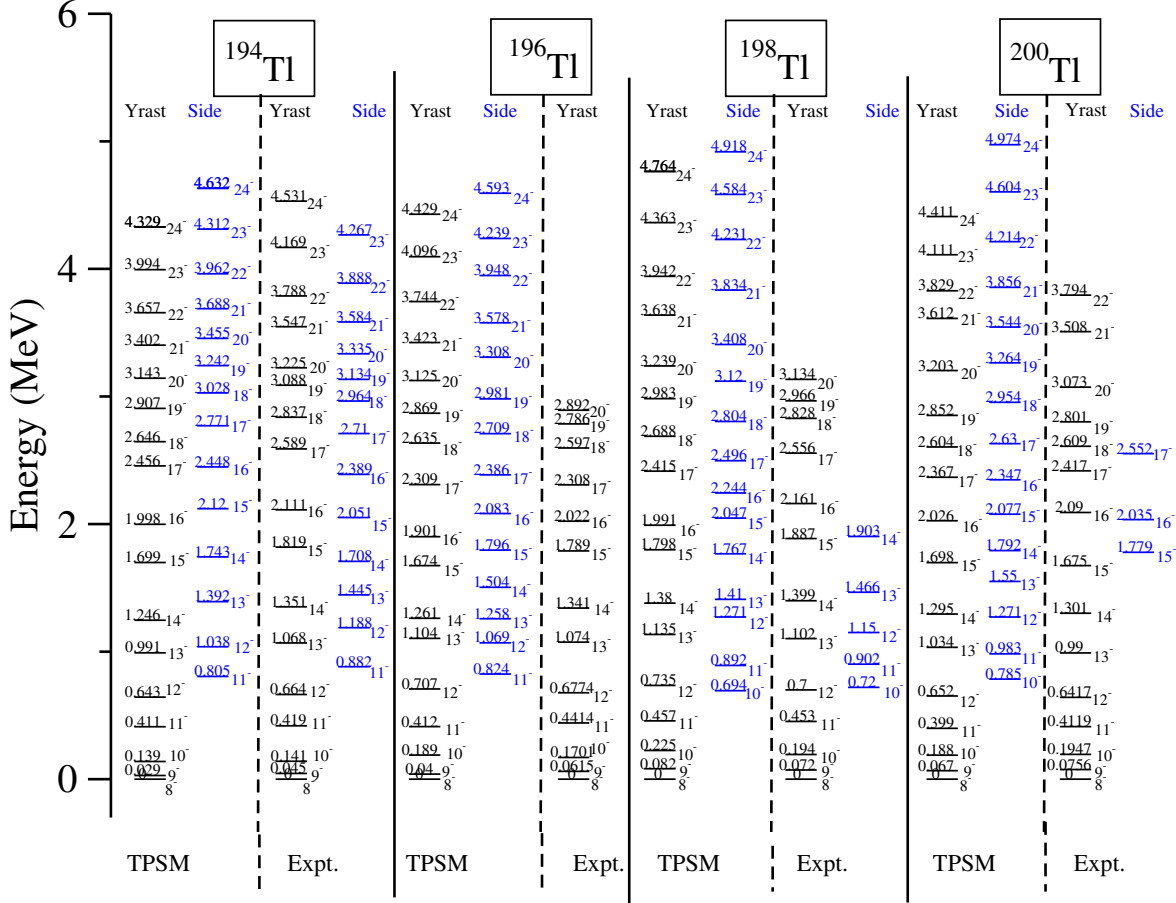


Fig. 2 (Color online) Comparison of experimental and the TPSM calculated energies for $^{194,196,198,200}\text{Tl}$ isotopes. Experimental results are from Refs. [3,4,5,6].

the yrast and the side band, and it is seen from the results that TPSM reproduces the measured ratios quite well, except at $I=23$ for the yrast and at $I=14$ for the side band. The experimental ratios are not available for ^{196}Tl and the TPSM ratios depict similar behaviour as that for ^{194}Tl . The ratios available for ^{198}Tl , shown in Fig. 9, are again noted to be in good agreement with the predicted values. The calculated TPSM ratios for ^{200}Tl are seen to deviate considerably from the experimental ratios at high spin. The experimental numbers depict a considerable drop with spin which is not observed in the TPSM values. The reason for this discrepancy could be due to fixed mean-field employed in the TPSM approach for all the calculated spin values, which obviously is unrealistic.

Though difficult to measure experimentally, we have calculated, using the TPSM wavefunctions, transitions between

the doublet bands and the corresponding mixing ratios, and are displayed in Figs. 10 and 11, respectively. It has been shown in a model study [8] that these transitions follow special selection rules for nuclei exhibiting chiral geometry. In Fig. 10, it is evident that inter-band $B(M1, I \rightarrow I)$ and $B(M1, I \rightarrow I-1)$ transitions have opposite phases for $^{194,196}\text{Tl}$ -isotopes, which has been predicted in the model study as one of the characteristic features of the chiral symmetry. It is noted that mixing ratios are also measured [42] for chiral bands as $M1$ and $E2$ transitions compete and are provided in Fig. 11 for comparisons with future experimental measurements.

As mentioned in the introduction, it has been speculated [3,4,5,6] that the doublet band structures observed in Tl-isotopes could be a result of the chiral symmetry breaking mechanism. Chiral symmetry has been identified in many

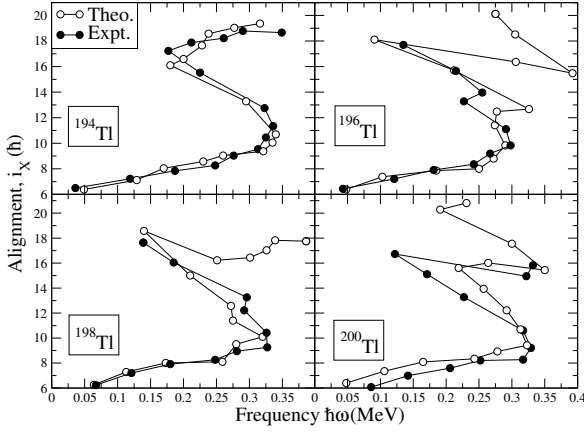


Fig. 3 (Color online) Comparison of experimental and the calculated alignment I_x as a function of rotational frequency $\hbar\omega$ for the yrast bands of odd-odd $^{194-200}\text{Tl}$ isotopes. The Harris reference parameters are taken as $J_0 = 8\hbar^2\text{MeV}^{-1}$ and $J_1 = 40\hbar^4\text{MeV}^{-3}$ [5].

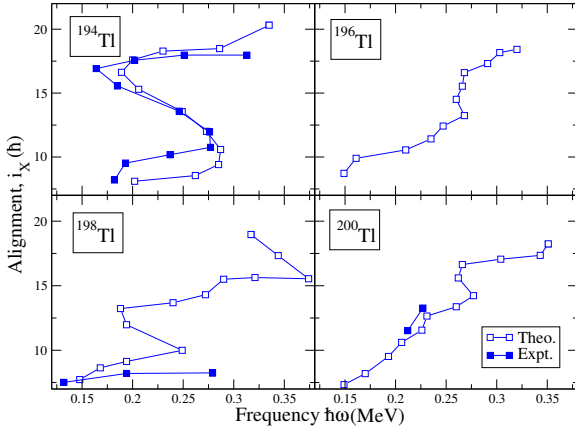


Fig. 4 (Color online) Comparison of experimental and the calculated alignment I_x as a function of rotational frequency $\hbar\omega$ for the side bands of odd-odd $^{194-200}\text{Tl}$ isotopes. The Harris reference parameters are taken as $J_0 = 8\hbar^2\text{MeV}^{-1}$ and $J_1 = 40\hbar^4\text{MeV}^{-3}$ [5].

of the regions of the periodic table and occurs in triaxially deformed systems with the angular momentum of valence protons, valence neutrons, and that of the core aligned along three orthogonal axis of the rotating nucleus. This leads to doublet bands with identical spectroscopic properties. In order to investigate the possibility of chiral symmetry breaking as the underpinning mechanism behind the emergence of doublet bands in Tl-isotopes, we have evaluated the theoretical and experimental differences of the energies and the transition probabilities between the doublet bands in each of the three isotopes. The difference in the transition probabilities is defined as [43]

$$\delta(\lambda\mu; I_i) = \frac{A-B}{A+B}, \quad (12)$$

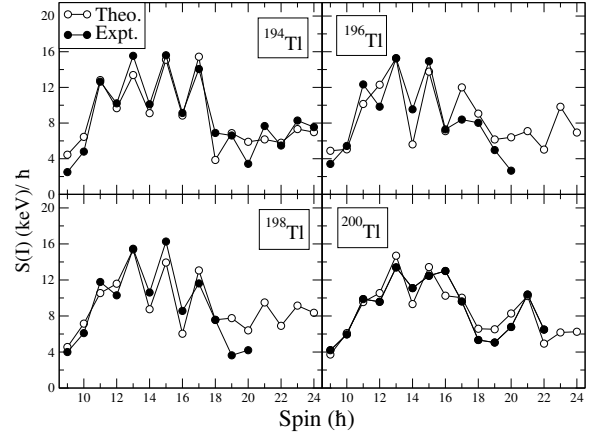


Fig. 5 (Color online) Comparison of experimental and the calculated staggering $[S(I) = (E(I) - E(I-1))/2I]$ for the yrast bands of odd-odd $^{194-200}\text{Tl}$ isotopes.

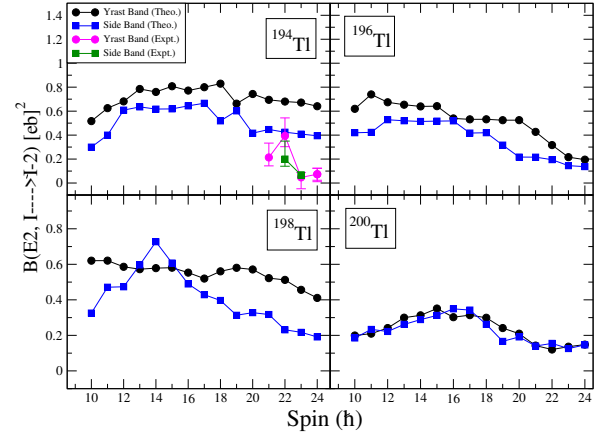


Fig. 6 (Color online) TPSM Calculated values of $B(E2, I \rightarrow I-2)$ (e^2b^2) for $^{194-200}\text{Tl}$ isotopes.

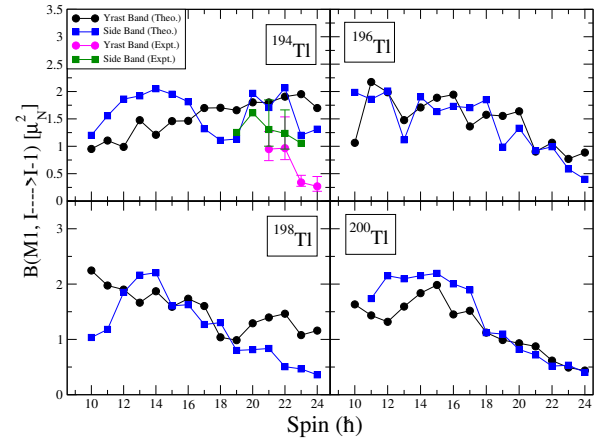


Fig. 7 (Color online) TPSM Calculated values of $B(M1, I \rightarrow I-1)$ (μ_N^2) for $^{194-200}\text{Tl}$ isotopes.

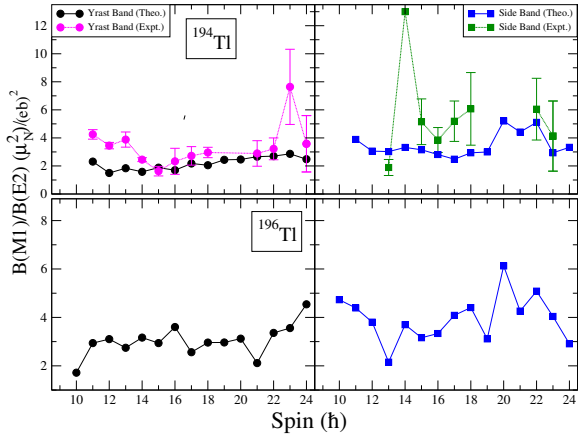


Fig. 8 (Color online) Comparison of experimental and the calcul $B(M1)/B(E2)$ for $^{194,196}\text{Tl}$ isotopes. Experimental results are fi Refs. [4,6].

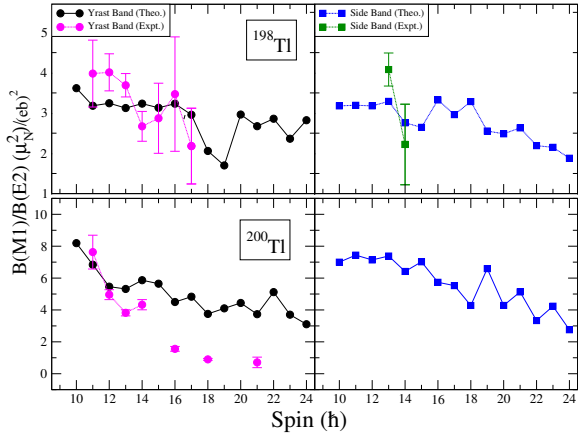


Fig. 9 (Color online) Comparison of experimental and the calcul $B(M1)/B(E2)$ for $^{198,200}\text{Tl}$ isotopes. Experimental results are fi Refs. [4,6].

where,

$$A = \sqrt{(2I_i + 1)B_{yrast}(\lambda\mu; I_i \rightarrow I)},$$

$$B = \sqrt{(2I_i + 1)B_{side}(\lambda\mu; I_i \rightarrow I)}.$$

It is expected that in the chiral symmetry breaking limit, the differences of the calculated properties for the doublet bands should tend to zero. The differences in the level energies $[\delta E]$, BE2 $[\delta E(2)]$ and BM1 $[\delta M(1)]$ are shown in Figs. 12, 13 and 14, respectively. For ^{194}Tl , both TPSM and the experimental $\delta(E)$ tend to zero with increasing spin, in particular, after the band crossing at $I=18$. It has been postulated in the earlier work that four-quasiparticle band structures, observed after the band crossing, could be the candidate chiral bands [4]. It is evident from Fig. 12 that for ^{194}Tl , $\delta(E)$ does, indeed, tend to zero. For other studied Tl-isotopes, the side bands have not been observed after the band crossing. However, the TPSM calculated differences

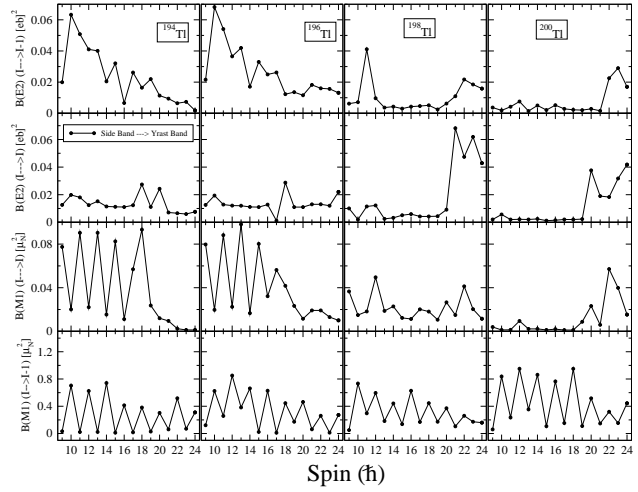


Fig. 10 (Color online) Calculated $B(E2)(I \rightarrow I - 1)$, $B(E2)(I \rightarrow I)$, $B(M1)(I \rightarrow I)$ and $B(M1)(I \rightarrow I - 1)$ for $^{194-200}\text{Tl}$ isotope from Side Band to Yrast Band.

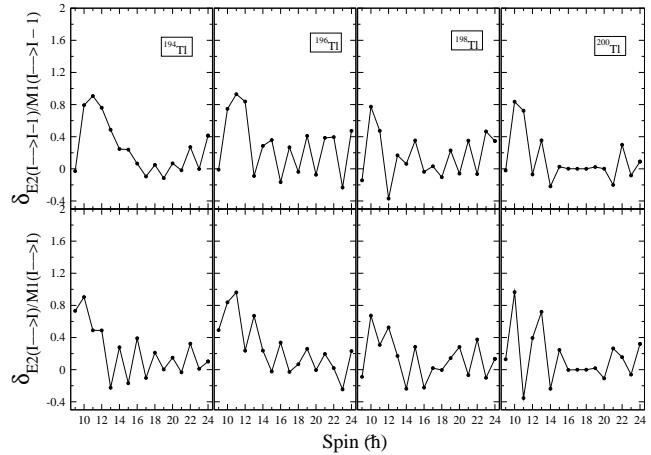


Fig. 11 (Color online) Mixing ratios for $^{194-200}\text{Tl}$ isotopes, calculated from the transitions given in Fig. 10 and using the expression $\delta_{E2/M1} = 0.835 E_\gamma \frac{\langle J_f || E2 || I_i \rangle}{\langle J_f || M1 || I_i \rangle}$ [44,45].

indicate that ^{198}Tl could possibly be another candidate of chiral symmetry breaking. In the case of ^{196}Tl and ^{200}Tl isotopes, the calculated $\delta(E)$, as a matter of fact, diverges after the bandcrossing and, therefore, chiral symmetry can be ruled out for these two isotopes. However, we would like to caution that these differences could also be an artifact of the model calculations and more experimental and theoretical studies are required to make firm conclusions.

The calculated differences in the transition probabilities, shown in Figs. 13 and 14, although small in all the cases, but tend to deviate for high spin states in ^{194}Tl , ^{196}Tl and ^{198}Tl

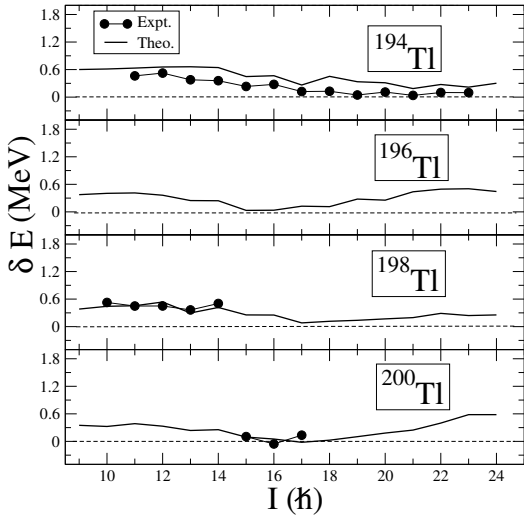


Fig. 12 (Color online) Comparison of experimental and the calculated Energy difference, $\delta(E)$, between doublet bands as a function of spin.

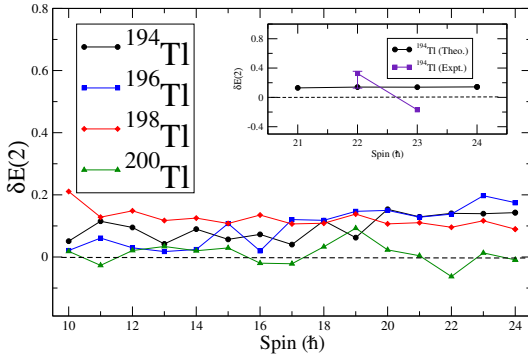


Fig. 13 (Color online) TPSM calculated values of $\delta(E2)$ as a function of spin.

isotopes. For ^{200}Tl , the deviations somewhat oscillate about the dashed zero line. In the chiral limit, these deviations are expected to approach zero with spin.

In a more recent experimental work [46], another negative parity dipole band has been reported along with the previously known two chiral partner bands. The measured transition probabilities reported in this work provide some details on the nature of the third observed band. This band has also been assigned to be built on the $\pi h_{9/2} \otimes \nu i_{13/2}^{-3}$ configuration, similar to the other two observed bands. Many particle rotor model (MPRM) calculations [46] suggest that the band 3 could be one partner of the second chiral pair bands in ^{194}Tl . The results of the MPRM model predict that the yrare partner of the first chiral pair and the both the bands of the second chiral pair have almost similar excitation energies. This predicted near degeneracy and the fact that these

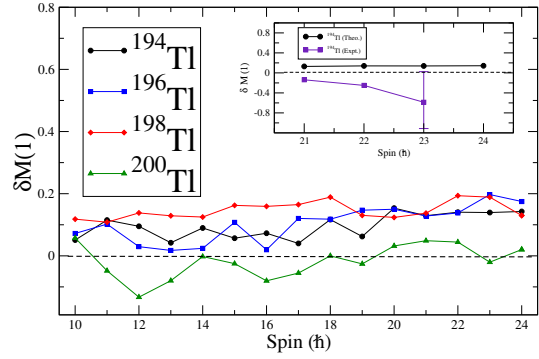


Fig. 14 (Color online) TPSM calculated values of $\delta(M1)$ as a function of spin.

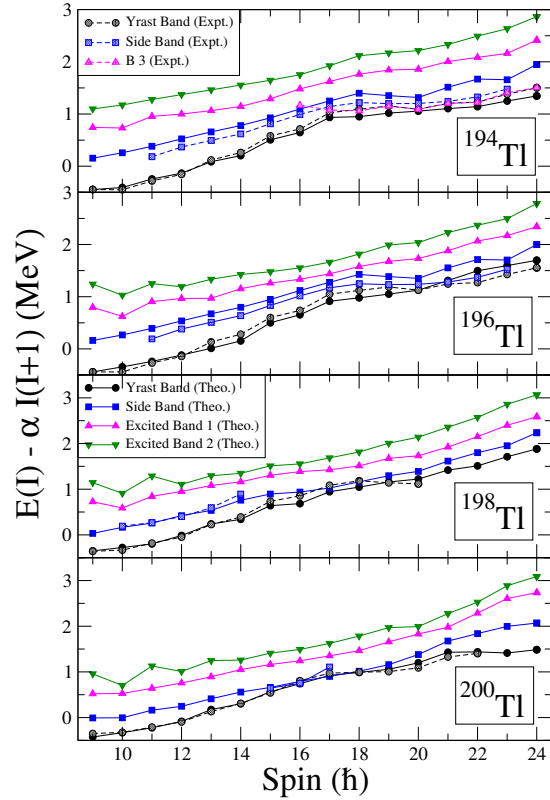


Fig. 15 (Color online) Comparison of the measured energy levels of negative parity yrast and excited bands for $^{194-200}\text{Tl}$ isotopes. The value of α , shown in y-axis, is defined as $\alpha = 32.32A^{-5/3}$.

bands are weakly populated, being non-yrast, could be the reason that the partner band of the second chiral pair has not been observed experimentally.

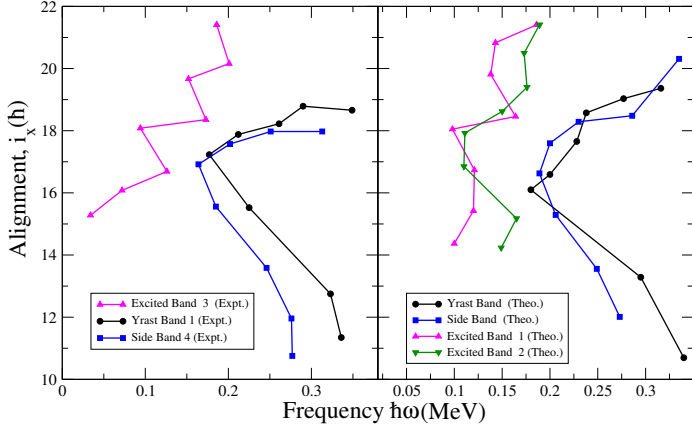


Fig. 16 (Color online) Comparison of experimental and the calculated alignment I_x as a function of rotational frequency $\hbar\omega$ for the bands 3, 1 and 4 of ^{194}Tl isotopes. The Harris reference parameters are taken as $J_0 = 8\hbar^2\text{MeV}^{-1}$ and $J_1 = 40\hbar^4\text{MeV}^{-3}$. Data is taken from Ref. [46].

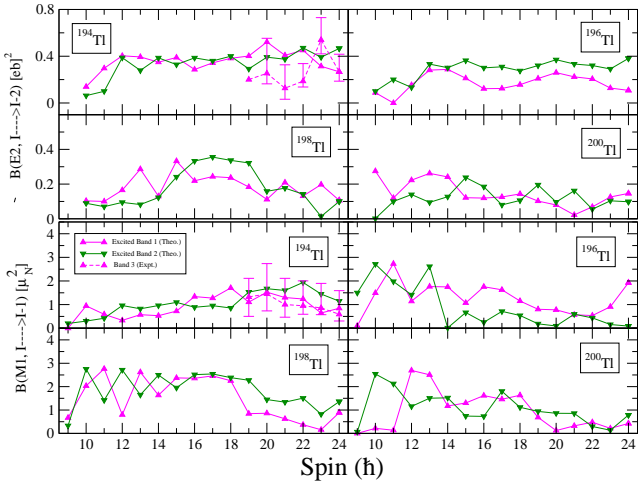


Fig. 17 (Color online) Calculated $B(E2)(I \rightarrow I - 2)$ and $B(M1)(I \rightarrow I - 1)$ for $^{194-200}\text{Tl}$ isotopes. Experimental Data for ^{194}Tl isotope is from Ref. [46].

The energies of the lowest four bands using the TPSM approach for the odd-odd Tl-isotopes studied in this work are depicted in Fig. 15. It is evident from these results that third and fourth bands are close on energy and could be due to the second chiral pair as predicted in MPRM study [46]. However, it is known that in odd-odd nuclei density of states is higher and the near degeneracy of the bands could just be as a results of it. In order to shed some light on the nature of the third observed band in ^{194}Tl , the alignments of the four bands, calculated using the TPSM approach, are compared with those deduced from the observed energies of the three known bands in Fig. 16. The alignment for the third

observed band is in close agreement with the alignment of the third excited band predicted in the TPSM approach. In the experimental work, the third band becomes lower in energy than that of yrare at higher spin.

The calculated $B(E2)$ and $B(M1)$ values for the excited two bands in the studied Tl-isotopes are shown in Fig. 17. It is quite evident from the figure that transitions are very similar for the two bands and may correspond to the excited chiral pairs. For ^{194}Tl , the measured values for few spin states are in good agreement with the calculated values. Clearly, further investigations are required to understand the excited band structures in Tl-isotopes.

4 Summary and Conclusions

In the present work, the TPSM approach for odd-odd nuclei has been generalized to include two-neutron and two-proton quasiparticle states coupled to the basic one-neutron \otimes one-proton. This allows to investigate odd-odd nuclei beyond the first band crossing, which is delayed as compared to even-even systems due to blocking of the orbitals by the unpaired particles. In odd-odd $^{194-200}\text{Tl}$ isotopes, high-spin states have been observed beyond the first band crossing and it has been proposed that the doublet bands observed in some of these isotopes may be a result of chiral symmetry breaking mechanism.

The generalized TPSM approach has been employed to investigate odd-odd $^{194-200}\text{Tl}$ isotopes and it has been shown that results are in fair agreement with the experimental data, wherever available. The energy differences for $^{194,200}\text{Tl}$ tend to drop with increasing spin and lends support to the conjecture that this near degeneracy may be due to the chiral symmetry breaking mechanism. However, the results of the transition probabilities, calculated using the TPSM approach, deviate from those expected in the chiral symmetry limit. It is, therefore, important to perform the lifetime measurements of the doublet bands in order to ascertain the true structure of these bands.

We would like to add that in a parallel effort [47,48,49], TPSM approach has been extended to include more than four-quasiparticles states and also K- and azimuthal- plots have been proposed to probe the chiral nature of the doublet bands. It would be quite interesting to extend such analysis to the Tl-isotopes studied in the present work.

ACKNOWLEDGEMENTS

Three of us (GHB, JAS and NR) would like to acknowledge DST for Project No.CRG/2019/004960 (Govt. of India) for providing the financial support to carry out the research work. The authors would also like to acknowledge Dr. E.A.

Lawrie and Dr. S. Bhattacharya for providing the measured data on the electromagnetic transitions for $^{194,200}\text{Tl}$ isotopes.

References

1. A. Bohr and B. R. Mottelson, *Nuclear Structure*, Vol. II (Benjamin Inc., New York, 1975).
2. D. J. Rowe and J. L. Wood, *Fundamentals of Nuclear Models: Foundational Models*, (World Scientific, 2010).
3. Soumik Bhattacharya, S. Bhattacharyya, S. Das Gupta, H. Pai, G. Mukherjee, R. Palit, F. R. Xu, Q. Wu, A. Shrivastava, Md. A. Asgar, R. Banik, T. Bhattacharjee, S. Chanda, A. Chatterjee, A. Goswami, V. Nanal, S. K. Pandit, S. Saha, J. Sethi, T. Roy, and S. Thakur, *Phys. Rev. C* **95** (2017) 014301.
4. P. L. Masiteng, E. A. Lawrie, T. M. Ramashidzha, R. A. Bark, B. G. Carlsson, J. J. Lawrie, R. Lindsay, F. Komati, J. Kau, P. Maine, S. M. Maliage, I. Matamba, S. M. Mullins, S. H. T. Murray, K. P. Mutshena, A. A. Pasternak, I. Ragnarsson, D. G. Roux, J. F. Sharpey-Schafer, O. Shirinda, P. A. Vymers, *Phys. Lett. B* **719** (2013) 83.
5. H. Pai, G. Mukherjee, S. Bhattacharyya, M. R. Gohil, T. Bhattacharjee, and C. Bhattacharya, R. Palit, S. Saha, J. Sethi, T. Trivedi, Shital Thakur, B. S. Naidu, S. K. Jadav, and R. Donthi, A. Goswami, S. Chanda, *Phys. Rev. C* **85** (2012) 064313.
6. E. A. Lawrie, P. A. Vymers, J. J. Lawrie, Ch. Vieu, R. A. Bark, R. Lindsay, G. K. Mabala, S. M. Maliage, P. L. Masiteng, S. M. Mullins, S. H. T. Murray, I. Ragnarsson, T. M. Ramashidzha, C. Schuck, J. F. Sharpey-Schafer, and O. Shirinda, *Phys. Rev. C* **78** (2008) 021305(R).
7. S. Frauendorf, *Rev. Mod. Phys.* **73** (2001) 463.
8. T. Koike, K. Starosta, and I. Hamamoto, *Phys. Rev. Lett.* **17** (2004) 172502.
9. J. Meng and S. Q. Zhang, *J. Phys. G* **37** (2010) 064025.
10. J. Meng and P. Zhao, *Phys. Scr.*, **91** (2016) 053008.
11. S. Frauendorf and J. Meng, *Nucl. Phys. A* **617** (1997) 131.
12. C. Vaman, D. B. Fossan, T. Koike, K. Starosta, I. Y. Lee, and A. O. Macchiavelli, *Phys. Rev. Lett.* **92** (2001) 032501.
13. T. Koike, K. Starosta, C. J. Chiara, D. B. Fossan, and D. R. LaFosse, *Phys. Rev. C* **67** (2003) 044319.
14. K. Starosta, T. Koike, C. J. Chiara, D. B. Fossan, D. R. LaFosse, A. A. Hecht, C. W. Beausang, M. A. Caprio, J. R. Cooper, R. Krücken, J. R. Novak, N. V. Zamfir, K. E. Zyranski, D. J. Hartley, D. L. Balabanski, Jing-ye Zhang, S. Frauendorf, and V. I. Dimitrov, *Phys. Rev. Lett.* **86** (2001) 971.
15. A. A. Hecht, C. W. Beausang, K. E. Zyranski, D. L. Balabanski, C. J. Barton, M. A. Caprio, R. F. Casten, J. R. Cooper, D. J. Hartley, R. Krücken, D. Meyer, H. Newman, J. R. Novak, E. S. Paul, N. Pietralla, A. Wolf, N. V. Zamfir, Jing-Ye Zhang, and F. Dönau, *Phys. Rev. C* **63** (2001) 051302.
16. S. Zhu, U. Garg, B. K. Nayak, S. S. Ghugre, N. S. Pattabiraman, D. B. Fossan, T. Koike, K. Starosta, C. Vaman, R. V. F. Janssens, R. S. Chakravarthy, M. Whitehead, A. O. Macchiavelli, and S. Frauendorf, *Phys. Rev. Lett.* **91** (2003) 132501.
17. C. Liu, S. Y. Wang, R. A. Bark, S. Q. Zhang, J. Meng, B. Qi, P. Jones, S. M. Wyngaardt, J. Zhao, C. Xu, S. G. Zhou, S. Wang, D. P. Sun, L. Liu, Z. Q. Li, N. B. Zhang, H. Jia, X. Q. Li, H. Hua, Q. B. Chen, Z. G. Xiao, H. J. Li, L. H. Zhu, T. D. Bucher, T. Dinoko, J. Easton, K. Juhász, A. Kamblawe, E. Khaleel, N. Khumalo, E. A. Lawrie, J. J. Lawrie, S. N. T. Majola, S. M. Mullins, S. Murray, J. Ndayishimye, D. Negi, S. P. Noncolela, S. S. Ntshangase, B. M. Nyakó, J. N. Orce, P. Papka, J. F. Sharpey-Schafer, O. Shirinda, P. Sithole, M. A. Stankiewicz, and M. Wiedeking, *Phys. Rev. Lett.* **116** (2016) 112501.
18. B. W. Xiong and Y. Y. Wang, *At. Data Nucl. Data Tables*, **125** (2019) 193.
19. S. Y. Wang, B. Qi, L. Liu, S. Q. Zhang, H. Hua, X. Q. Li, Y. Y. Chen, L. H. Zhu, J. Meng, S. M. Wyngaardt, P. Papka, T. T. Ibrahim, R. A. Bark, P. Datta, E. A. Lawrie, J. J. Lawrie, S. N. T. Majola, P. L. Masiteng, S. M. Mullins, J. Gál, G. Kalinka, J. Molnár, B. M. Nyakó, J. Timár, K. Juhász, and R. Schwengner, *Phys. Lett. B* **703** (2011) 40.
20. T. Roy, G. Mukherjee, Md. A. Asgar, S. Bhattacharyya, S. Bhattacharya, C. Bhattacharya, S. Bhattacharya, T. K. Ghosh, K. Banerjee, S. Kundu, T. K. Rana, P. Roy, R. Pandey, J. Meena, A. Dhal, R. Palit, S. Saha, J. Sethi, S. Thakur, B. S. Naidu, S. V. Jadav, R. Dhonti, H. Pai, A. Goswami, *Phys. Lett. B* **782** (2018) 768.
21. S. J. Zhu, J. H. Hamilton, A. V. Ramayya, P. M. Gore, J. O. Rasmussen, V. Dimitrov, S. Frauendorf, R. Q. Xu, J. K. Hwang, D. Fong, L. M. Yang, K. Li, Y. J. Chen, X. Q. Zhang, E. F. Jones, Y. X. Luo, I. Y. Lee, W. C. Ma, J. D. Cole, M. W. Drigert, M. Stoyer, G. M. Ter-Akopian, and A. V. Daniel, *Eur. Phys. J. A* **25** (2005) 459.
22. V. I. Dimitrov, S. Frauendorf, and F. Dönau, *Phys. Rev. Lett.* **84** (2000) 5732.
23. P. Olbratowski, J. Dobazewski, J. Dudek, and W. Plöciennik, *Phys. Rev. Lett.* **93** (2004) 052501.
24. S. Q. Zhang, B. Qi, S. Y. Wang, and J. Meng, *Phys. Rev. C* **75** (2007) 044307.
25. S. Mukhopadhyay, D. Almeded, U. Garg, S. Frauendorf, T. Li, P. V. Madhusudhana Rao, X. Wang, S. S. Ghugre, M. P. Carpenter, S. Gros, A. Hecht, R. V. F. Janssens, F. G. Kondev, T. Lauritsen, D. Seweryniak, and S. Zhu, *Phys. Rev. Lett.* **99** (2007) 172501.
26. D. Almeded, F. Dönau, and S. Frauendorf, *Phys. Rev. C* **83** (2011) 054308.
27. J. A. Sheikh and K. Hara, *Phys. Rev. Lett.* **82** (1999) 3968.
28. G. H. Bhat, J. A. Sheikh, and R. Palit, *Phys. Lett. B* **707** (2012) 250.
29. G. H. Bhat, R. N. Ali, J. A. Sheikh, and R. Palit, *Nucl. Phys. A* **922** (2014) 150.
30. W. A. Dar, J. A. Sheikh, G. H. Bhat, R. Palit, R. N. Ali, and S. Frauendorf, *Nucl. Phys. A* **933** (2015) 123.
31. C. L. Zhang, G. H. Bhat, W. Nazarewicz, J. A. Sheikh and Y. Shi, *Phys. Rev. C* **92** (2015) 034307.
32. G. H. Bhat, J. A. Sheikh, Y. Sun, and R. Palit *Nucl. Phys. A* **947** (2016) 127.
33. J. A. Sheikh, G. H. Bhat, W. A. Dar, S. Jehangir and P. A. Ganai, *Phys. Scr.* **91** (2016) 063015.
34. P. Ring and P. Schuck, *The Nuclear Many-Body Problem* (Springer, New York, 1980).
35. K. Hara and S. Iwasaki, *Nucl. Phys. A* **332** (1979) 61.
36. K. Hara and S. Iwasaki, *Nucl. Phys. A* **348** (1980) 200.
37. S. G. Nilsson, C. F. Tsang, A. Sobczewski, Z. Szymanski, S. Wycech, C. Gustafson, I. Lamm, P. Moller, B. Nilsson, *Nucl. Phys. A* **131**, 1 (1969).
38. K. Hara and Y. Sun, *Int. J. Mod. Phys. E* **4** (1995) 637.
39. J. -Ye Zhang, A. J. Larabee and L. L. Riedinger, *J. Phys. G* **13** (1987) 75.
40. Y. Sun and J. L. Egido, *Nucl. Phys. A* **580** (1994) 1.
41. N. Tajima, *Nucl. Phys. A* **572** (1994) 365.
42. S. Zhu, U. Garg, B. K. Nayak, S. S. Ghugre, N. S. Pattabiraman, D. B. Fossan, T. Koike, K. Starosta, C. Vaman, R. V. F. Janssens, R. S. Chakravarthy, M. Whitehead, A. O. Macchiavelli, and S. Frauendorf, *Phys. Rev. Lett.* **91** (2003) 132501.
43. E. Grodner, *Acta Physica Polonica B* **39** (2008) 531.
44. F. Dönau and S. Frauendorf in 'Proceedings of the International Conference on High. Angular Momentum Properties of Nuclei', Oak Ridge (July 1982), *Nucl. Sci.*
45. A. Gsannatempo, G. Maino, A. Nannini, and P. Sona, *Phys. Rev. C* **48** (1993) 6.
46. P. L. Masiteng, A. A. Pasternak, E. A. Lawrie, O. Shirinda, J. J. Lawrie, R. A. Bark, S. P. Bvumbi, N. Y. Kheswa, R. Lindsay, E. O. Lieder, R. M. Lieder, T. E. Madiba, S. M. Mullins, S. H. T. Murray, J. Ndayishimye, S. S. Ntshangase, P. Papka, and J. F. Sharpey-Schafer, *Eur. Phys. J. A* **52** (2016) 28.

-
47. F. Q. Chen, Q. B. Chen, Y. A. Luo, J. Meng, and S. Q. Zhang, Phys. Rev. C **96** (2017) 051303.
 48. F. Q. Chen, J. Meng, and S. Q. Zhang, Phys. Lett. B **785** (2018) 211.
 49. Y. K. Wang, F. Q. Chen, P. W. Zhao, S. Q. Zhang, and J. Meng, Phys. Rev. C **99** (2019) 054303.